Low-Profile Wideband MetasurfaceAntenna with Polarization Reconfiguration via Resistor Control and Reduced RCS for Enhanced Wireless Communication

Zhendong Ding, Jiawang Li, Dan Zhang, Michael Yan-Wah Chia, Hao Wang, Nasimuddin Nasimuddin

***Abstract*—This paper presents a low-profile, single-layer, broadband, polarization-reconfigurable metasurface antenna with a low radar cross section(RCS), designed using characteristic mode analysis(CMA) for a staggered elliptical-shaped unit cell metasurface. The staggered arrangement of the elliptical metasurface structures, oriented at 90° , facilitates mode fusion through CMA to effectively reduce RCS. The analysis of a defective floor with branching reveals a characteristic angle (CA) relationship of 90° , which is critical for generating circular polarization (CP) waves. Experimental measurements indicate that the fabricated antenna achieves a -10 dB impedance bandwidth(IBW) from 5.5 GHz to 8.3 GHz, (40.6%). It also demonstrates a 3dB axial ratio bandwidth (ARBW) from 6.3 GHz to 8.2 GHz, equivalent to 26.2%. The antenna exhibits a peak gain of 5.1 dBi at 6.3 GHz. By incorporating resistors, the antenna enables switching between CP and linear polarization (LP), as well as between different frequency bands, resulting in three distinct operating states. Furthermore, a monostatic RCS reduction of the metasurface structure is achieved across the frequency range of 2.0 GHz to 22.0 GHz, yielding a significant reduction of 166.7%, and a 6 dBsm reduction in RCS within the impedance bandwidth from 6.3 GHz to 7.2 GHz.**

***Index Terms* — Characteristic-mode analysis, reconfigurable, circular polarization, metasurface, low radar cross section.**

I. Introduction

As wireless communication systems become more advanced, the need to integrate multiple subsystems on a single platform has grown. This integration often requires an increasing number of antennas, which can lead to several challenges, including higher system costs, larger form factors, and electromagnetic interference between antennas. These issues not only impact on the overall operation of the system but can also lead to malfunctions. Addressing these challenges is crucial for the future development of efficient and reliable wireless communication technologies. Therefore, the design of antennas has become a major bottleneck that restricts the development and application of wireless communication systems towards high-capacity, multifunctional, and wideband directions [1]-[5]. To overcome the constraints of antennas on the development of wireless communication technology and enable antennas to adapt to the multifunctional requirements of systems and complex and diverse application scenarios, the application of reconfigurable antenna technology has emerged. Reconfigurable antenna [6]-[8] is a type of antenna that artificially changes the antenna size, or the distribution of the antenna aperture field based on the application state of the antenna electrical parameters, while ensuring that the electrical parameters remain basically unchanged, in order to achieve the basic unchanged electrical characteristics such as antenna operating frequency, directional pattern, polarization, etc. Therefore, reconfigurable antennas have strong vitality as a new type of antenna for communication systems.

Reconfigurable antennas can dynamically adjust the aperture or feeding structure of antenna radiation elements using electrical, optical, mechanical, and other means to change their working characteristics in real time. They can independently control their frequency characteristics, radiation patterns, and polarization modes, achieving multiple functions for one antenna. Reconfigurable-antennas can be categorized based on their reconstruction performance into several types: frequency [9]-[13], polarization [14]-[18], pattern [19]-[23], and hybrid reconfigurable-antennas [24]-[28]. Among them, hybrid reconfigurable are antennas that can control two or three types of performance, such as frequency/pattern, frequency/polarization, and pattern/polarization reconfigurable antennas, etc. For frequency reconfigurable across different bands, various implementations have achieved notable results: two capacitors enabled five states [9], six diodes achieved thirty-six states [10], sixteen diodes provided two states [11], three diodes realized six states [12], and three diodes achieved four states [13]. In terms of polarization reconfigurability, numerous studies have demonstrated impressive capabilities: six diodes facilitated the conversion from LP to CP [14]. A dielectric resonator enabled the switch from horizontal polarization (HP) to vertical polarization (VP) [15]. Two diodes allowed transitions between left-handed circularly polarized(LHCP), right-handed circularly-polarized(RHCP), and LP [16, 17]. Additionally, twelve diodes enabled switching among HP, VP, LHCP, and RHCP [18]. For radiation pattern reconfigurability, two diodes

This work was supported in part by the Postgraduate Research & Practice Innovation Program of Jiangsu Province in China (KYCX23_0467). (*Corresponding author: Hao Wang.*)

Z. Ding, and H. Wang are with the School of Electronic and Optical Engineering, Nanjing University of Science and Technology, Nanjing 210094, China (e-mail: dingzhendong@njust.edu.cn, haowang@njust.edu.cn).

J. Li is with the School of Information Science and Engineering, Southeast University, Nanjing 210096, China (e-mail: jiawangli9999@gmail.com).

D. Zhang is with the College of Information Science and Technology, Nanjing Forestry University, Nanjing 210037, China (zhangdan@njfu.edu.cn). Nasimuddin and M. Y.-W. Chia are with the Institute for Infocomm Research, A*STAR, Singapore 138632 (e-mail: nasimuddin@i2r.a-star.edu.sg, michael_chia@i2r.a-star.edu.sg).

achieved both directional and dual-beam patterns [19], while four diodes produced directional and omnidirectional patterns [20]. A combination of two resistors, three capacitors, and four diodes yielded directional radiation patterns at low frequencies and bidirectional as well as directional patterns at high frequencies [21]. Furthermore, two graphene nanoplate pads facilitated directional and dual-beam patterns [22], and six diodes achieved narrow and wide beam patterns [23].

From the perspective of the reconfigurable technology of the implemented antenna, there are mainly the following solutions: loading RF switches, such as PIN diode, FET transistor, and MEMS switches, which can effectively control frequency, polarization, and radiation patterns, 2) Loading a varactor diode, using a varactor diode can easily achieve continuous adjustability of the operating frequency, 3) Resistors can also be used to control frequency and polarization, 4) adjust the mechanical structure of the antenna, the material properties of the antenna, and through optical switches. In fact, the specific reconfiguration of its performance depends on the location where these control devices are connected with the antenna structure. In addition to introducing devices to achieve reconfigurable technology in gaps, patches, and feed network structures, few reconfigurable papers that incorporate diodes on metasurfaces have been published in [29]-[31]. In addition, in terms of analysis methods, a polarization reconfigurable antenna has been designed to use CMA [32]. Some also use controllable liquid metal to achieve reconfigurable antenna performance [33]-[35].

In this paper, we present a low-profile, low-RCS single-layer broadband polarization reconfigurable antenna designed and measured using a CMA for staggered elliptical metasurfaces. The antenna structure features a defective ground plane, elliptical metasurfaces, a rectangular microstrip, and a coaxial feeding method. First, the defective ground plane is analyzed with CMA to establish a 90° circular alignment relationship, ensuring the generation of CP waves. Next, the staged elliptical metasurfaces structure is optimized to minimize RCS. Finally, resistors are strategically positioned to enable reconfigurable performance. The proposed antenna incorporates several advantages, including a simple structure, low profile, low RCS, cost-effectiveness, CP and LP capabilities, broadband performance, and ease of integration. Its operating frequency band is suitable for the C-band in modern wireless communications. The paper is planned as follows; Section 2 covers the analysis and design of the proposed antenna, detailing the geometric structure in Section 2.1, the CP mechanism and mode analysis in Section-2.2, and the designs and analysis of reconfiguration (Section 2.3). Section 3 presents the measurement results of the reconfigurable antenna and compares its performance with other related designs. Finally, Section 4 presents the conclusion.

II. Design and Analysis of Antenna

A. *The geometry structure of the proposed Antenna*

The proposed reconfigurable antenna is a single-layer substrate with the dielectric constant of ε_r = 2.65 and the tangent loss of tanδ = 0.0015. It consists of an elliptical patch metasurface, a rectangular microstrip patch, an F4B substrate, and a defective floor, with a simple structure and low cost. The elliptical metasurfaces are arranged at right angles, which helps to reduce RCS and generate CP waves. The defective branches and rectangular patches form a right-angle relationship, which is also a principal factor in radiating CP waves. After determining its structure, broadband and CP characteristics are generated, and then three resistors are introduced to connect at the defective ground, metasurface, and rectangular patch, forming the reconstruction characteristics. The structural optimization is analyzed and simulated using HFSS and CST software. The exploded view structure and dimensions of the polarization reconfigurable metasurface antenna is illustrated Fig. 1.

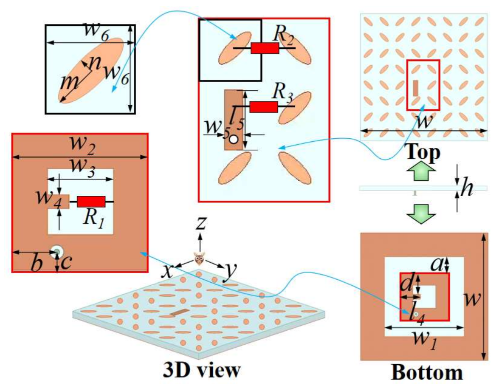

Fig. 1. The exploded view of low-profile wideband metasurface antenna with polarization reconfigurable: w = 80, w_1 = 50, w_2 = 30, w_3 = 14.4, w_4 = 3, l_4 = 12.5, w_5 = 3, l_5 = 10, w_6 = 10, a = 10, b = 9.8, c = 4, d = 13.5, h = 3, n = 1.2, m = 3.6. (all dimensions are in mm).

B. *The mechanism of the CP and mode analysis*

The CMT (characteristic mode theory) [36]-[38] describes a series of equally orthogonal characteristic modes for conductors of any shape, and these mutually orthogonal characteristic modes are essential properties of conductors that have convergence and completeness and can correctly characterize the solution to electromagnetic problems. The CMT has clear physical concepts and can provide a clear understanding of the working mechanism of electromagnetic structures. At the same time, the characteristic mode is only associated to the size, shape, and operational frequency of the electromagnetic structure, and is independent of external excitation, making it easy to guide engineering design. Considering its CP characteristics, we analyze a defective floor in relation to the proposed antenna design.

In the CMT, there are several physical quantities that can be used to analyze ideal conductors, namely CA (characteristic angle), MS (mode significance), and CC (characteristic current). MS can observe the resonance state of the conductor, with a range of [0,1]. When it is greater than 0.707, there is already a resonance bandwidth, and when it is equal to 1, it is the resonance point with strong resonance ability. The MS can be calculated as,

$$\mathrm{MS}_n = \left| \frac{1}{1 + j\lambda_n} \right| \tag{1}$$

where λ_n is the eigenvalue. From Fig. 2 (a), the defective ground plate has two modes that resonate in the observable range, with the other modes serving as auxiliary functions. Mode 4 resonates at 5.96 GHz with a resonance bandwidth of 5.19 GHz - 9 GHz, while Mode 5 resonates at 7.37 GHz with a resonance bandwidth of 6.58 GHz - 8.25 GHz.

CA can assist in analyzing the phase angle of CP. CA can be calculated as,

$$\mathrm{CA}_n = 180° - \tan^{-1}\lambda_n \tag{2}$$

At the intersection of two modes of MS, one can observe their characteristic angles. In Fig. 2(a), there are two frequency points with a characteristic angle difference of about 90 degrees, namely P1 and P2. They are at the intersection of Mode 1 and Mode 5 at 6.47 GHz (94.2° at P1), and at the intersection of Mode 5 and Mode 8 at 8.17 GHz (92.3° at P2). Because its two frequency points are close to 90°, with the assistance of other modes, it ensures that CP waves can be excited at two points. According to CMA, resonance can occur within the frequency band and may excite CP waves within the resonance band. Its impedance bandwidth is excited by the main mode, while the CP wave is excited by both the main mode and higher-order modes.

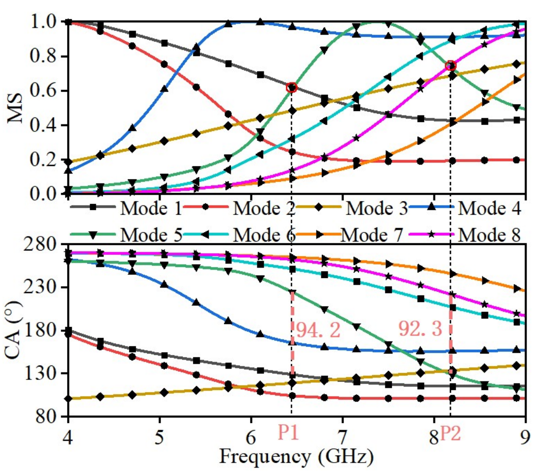

(a)

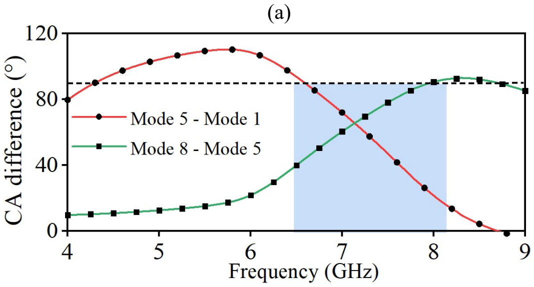

(b)

Fig. 2. The characteristic mode analysis of the defective ground: (a) MS and CA, and (b) CA difference.

Perform mode analysis on cell units with metasurface structures. All three combinations of MS structures can resonate in the observable frequency range in Fig. 3. Its arrangement is orthogonal, which requires CC analysis. The current direction is orthogonal, which is also the factor that ensures the generation of CP waves. Due to the orthogonality of the model, a pair of degenerate characteristic modes must be orthogonal. In Fig. 4, this pair of degenerate mode can be simultaneously excited to achieve CP characteristics.

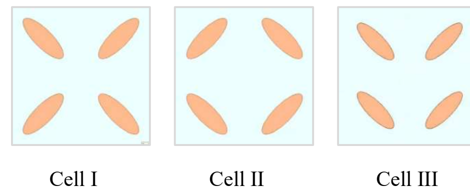

(a)

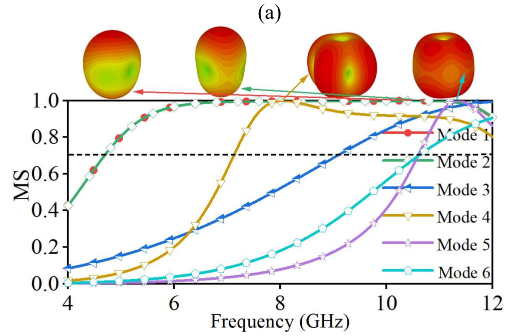

(b)

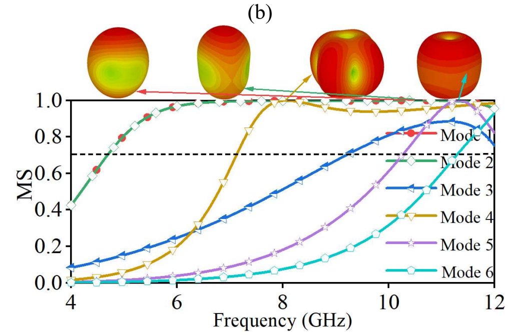

(c)

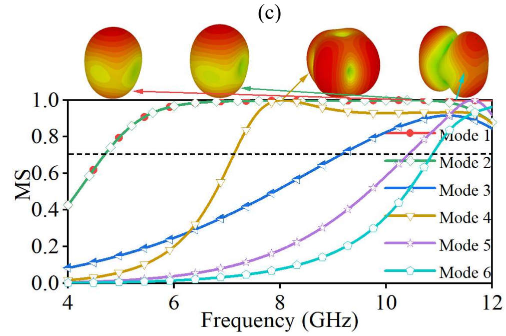

(d)

Fig. 3. The CMA of arranged cells: (a) three structures of cells (b) MS of cell I, (c) MS of cell II, and (d) MS of cell III.

When implementing CP characteristics, the direction of current is the key to observing whether it can excite CP waves. The antenna has added a 50 Ω SMA to excite a section of the transmission line in a coaxial manner. Observing the current on the ground and transmission lines of its defects, the distribution at 0° and 90° is orthogonal, and the current distribution on its metasurface is also almost orthogonal.

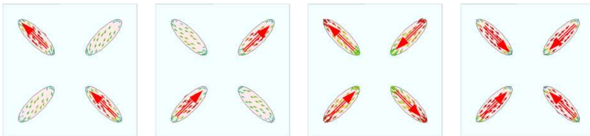

(a)

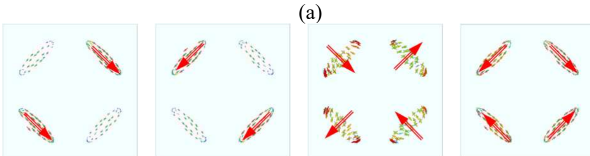

(b)

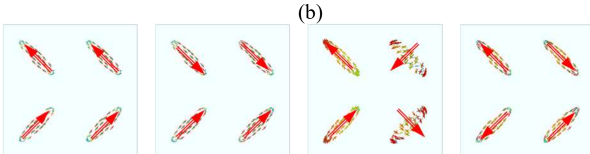

(c)

Fig. 4. Mode current at resonance points: (a) Mode #1, Mode #2, Mode #4 and Mode #5 at 10.61 GHz, 10.61 GHz, 8.05 GHz and 11.37 GHz respectively, (b) Mode#1, Mode#2, Mode#4 and Mode #5 at 10.64 GHz, 10.64 GHz, 8.06 GHz and 11.32 GHz respectively, and (c) Mode#1, Mode #2, Mode #4 and Mode #5 at 10.75 GHz, 10.75 GHz, 8.05 GHz and 11.62 GHz respectively.

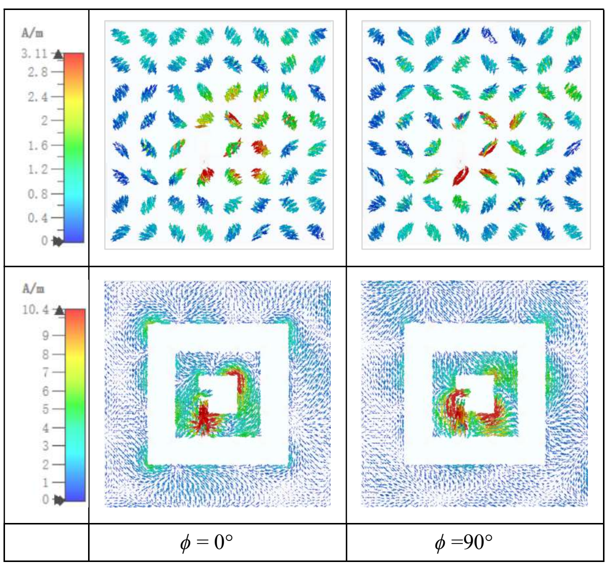

Fig. 5. Current distribution of the metasurface, defective ground and transmission line under two different phase conditions after excitation at 7 GHz.

However, at the same current intensity of 90°, the effect of the higher-order modes causes other current distributions, which is also a factor in the broadband generation of higher-order modes. The antenna has added a 50 Ω SMA to excite a section of the transmission line in a coaxial manner. Observing the current on the ground and transmission lines of its defects, the distribution at 0° and 90° is orthogonal, and the current distribution on its metasurface is also almost orthogonal. However, at the same current intensity of 90°, the effect of the higher-order modes causes other current distributions, which is also a factor in the broadband generation of higher-order modes. Therefore, the generation of CP waves requires two orthogonal horizontal and vertical electric fields with the same phase difference of 90°, namely,

$$E_{x0} = E_{y0} \tag{3}$$

$$E_x(t) = E_{x0}\cos(\omega t + \varphi_x) \tag{4}$$

$$\begin{aligned} E_y(t) &= E_{y0}\cos(\omega t + \varphi_y \pm \pi/2 + 2n\pi) \\ &= \pm E_{x0}\sin(\omega t + \varphi_x) \end{aligned} \tag{5}$$

When $|E_{x0}|=|E_{y0}|=E_0$, the orthogonal phase φ_x and φ_y satisfies the following relationship, indicating LHCP and RHCP,

$$\Delta\varphi = \varphi_x - \varphi_y = \begin{cases} +\pi/2(\text{RHCP}) \\ -\pi/2(\text{LHCP}) \end{cases} \tag{6}$$

After analysis, simulation, and optimization using CST and HFSS, the proposed metasurface CP antenna has achieved an IBW of 35.5% (5.8 GHz-8.3 GHz), an ARBW of 24.3% (6.5 GHz-8.2 GHz), and a maximum gain of 5.1 dBi at 6.3 GHz in Fig. 6. The IBW and ARBW correspond one-to-one with the MS and CA of CMA to validate the proposed analysis.

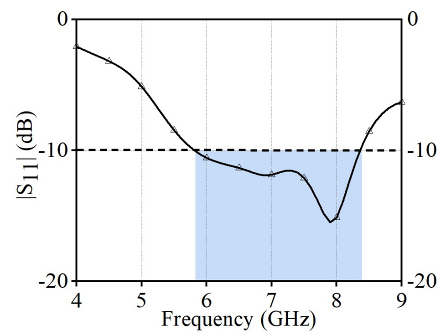

(a)

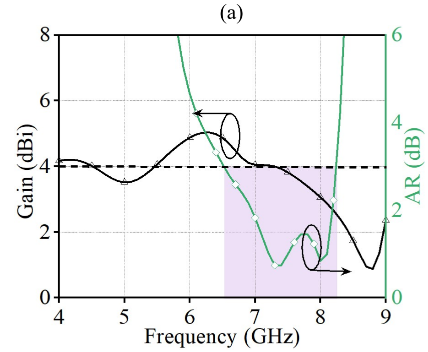

(b)

Fig. 6. The simulation results of the proposed CP metasurface antenna: (a) $|S_{11}|$, (b) gain and AR.

C. Design and analysis of reconfiguration

Considering the reconfigurable state of polarization, some resistors are connected near the strong current of the antenna, which can also achieve changes in impedance and current direction, thereby achieving a reconfigurable effect. Combining Fig. 1 and Fig. 5, three positions are selected to connect three resistors. Fig. 7 shows the equivalent circuit of the proposed reconstructed antenna. C_a and C_b represent the capacity generated by the groove on the metasurface of the ground. Therefore, resistors added to the reconfigurable circuit can replace capacitors. The total input impedance Z_{in} is

$$Y_a = \left[1/j\omega C_c + (1/R_a + j\omega C_a + 1/j\omega L_a)^{-1}\right]^{-1}$$
$$\text{or} \left[1/j\omega C_c + (1/R_a + 1/R_x + 1/j\omega L_a)^{-1}\right]^{-1} \quad (7)$$

$$Y_b = \left[1/j\omega C_d + (1/R_b + j\omega C_b + 1/j\omega L_b)^{-1}\right]^{-1}$$
$$\text{or} \left[1/j\omega C_d + (1/R_b + 1/R_x + 1/j\omega L_b)^{-1}\right]^{-1} \quad (8)$$

$$Z_{in} = 1/Y_{in} = 1/(Y_a + Y_b) \approx R + jX \quad (9)$$

The current distribution of the proposed circularly polarized (CP) antenna, relevant to changing the polarization state, is illustrated in Fig. 5. If a resistor is connected at the branch and slot, the direction of its current is different from the current state of the original model, and its polarization changes from CP to LP. Three positions of the antenna are connected with resistors to change the polarization state. State 2 involves adding a resistor between the branch and the slot, State 3 involves adding a resistor on the metasurface based on State 2, and State 4 involves adding a resistor between the metasurface and the rectangular patch based on State 3. Fig. 8 (a) - (b) show the comparison results of $|S_{11}|$, Gain, and AR with resistances of 100 Ω, 200 Ω, 300 Ω, and 400 Ω, respectively. Fig. 8 (c) - (d) show the comparison results of state 3. Fig. 8 (e) - (f) show the comparison results of state 4. Finally, the optimized results were determined to select resistors with resistance values of 100 Ω. The IBW of state 2 is 23.9% with a peak gain (PG) of 3.5 dBi at 6.7 GHz, the IBW of state 3 is 24.8% with a PG of 4.0 dBi at 6.8 GHz, and the IBW of state 4 is 24.1% with a PG of 4.8 dBi at 7.1 GHz. The maximum radiation efficiencies (RE) of states 1, 2, 3, and 4 are 92.1% at 8.0 GHz, 80.2% at 6.0 GHz, 79.2% at 7.5 GHz, and 74.5% at 6.5 GHz, respectively,

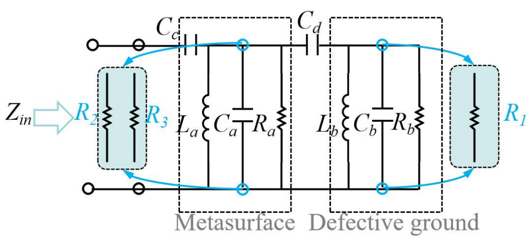

Fig. 7. The equivalent circuit of the proposed reconfigurable antenna.

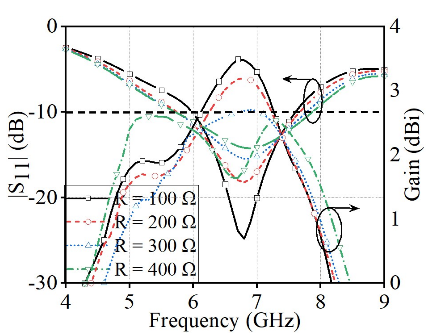

(a)

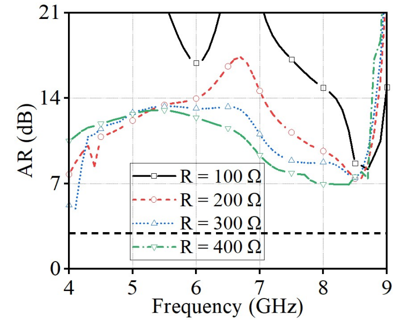

(b)

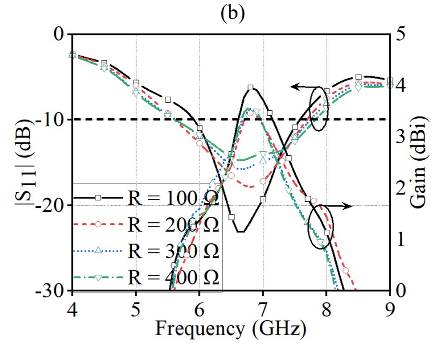

(c)

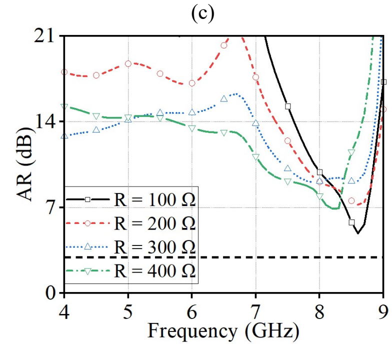

(d)

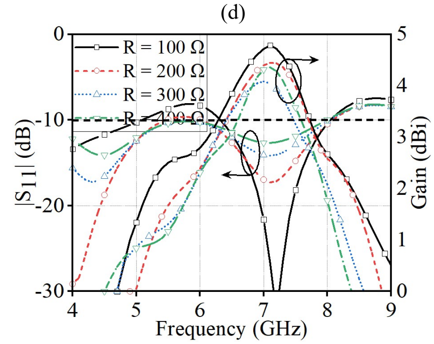

(e)

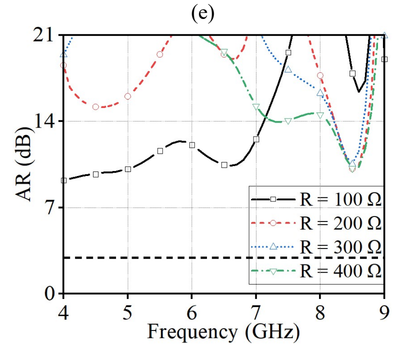

(f)

Fig. 8. Simulation results after adding resistors: (a) |S11| and gain in state 1, (b) AR in state 1, (c) |S11| and gain in state 2, (d) AR in state 2, (e) |S11| and gain in state 3, (f) AR in state 3.

TABLE I
SIMULATION RESULTS UNDER RESISTORS STATES

Device	State	Value (Ω)	Pol.	ARBW (%)	IBW (%)	PG (dBi)
No Resistors	State 1	/	CP	24.3	35.5	5.1
Resistors	State 2	R1 = 100	LP	/	23.9	3.5
	State 3	R1 = 100 R2 = 100	LP	/	24.8	4.0
	State 4	R1 = 100 R2 = 100 R3 = 100	LP	/	24.1	4.8

III. MEASUREMENT AND DISCUSSION

To validate the feasibility of the proposed reconfigurable antenna, it was fabricated and tested, as shown in Fig. 9. In the absence of resistors, the proposed CP metasurface antenna has a -10 dB 40.6% IBW (5.5 GHz - 8.3 GHz) and a 3-dB 26.2% ARBW (6.5 GHz - 8.2 GHz), with a PG of 5.1 dBi at 6.3 GHz Fig. 10 (a) - (b). After adding resistors, measurements were taken for states 2, 3, and 4 respectively. State 2 has 26.5% (5.9 GHz - 7.7 GHz) IBW and a PG of 3.4 dBi at 6.8 GHz in Fig. 10 (c). State 3 has 26.9% (5.8 GHz - 7.6 GHz) IBW and a PG of 3.8 dBi at 6.9 GHz in Fig. 10 (d). State 4 has 26.9% (6.2 GHz - 8.1 GHz) IBW and a PG of 4.7 dBi at 7.0 GHz in Fig. 10 (e).

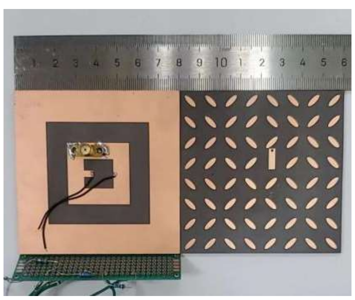

(a)

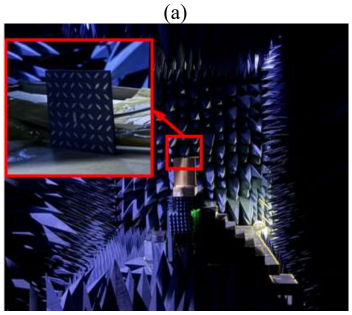

(b)

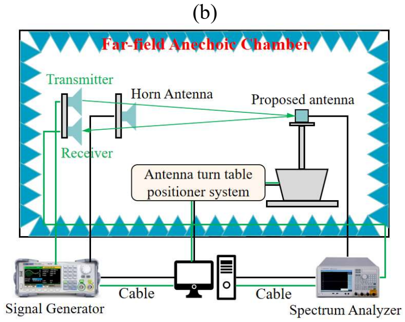

(c)

Fig. 9. Prototype and measurement of the proposed antenna: (a) Fabricated prototype, (b) Anechoic chamber for measurement, and (c) Anechoic chamber for radiation pattern and RCS measurement framework.

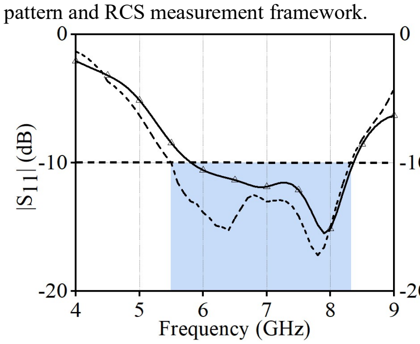

(a)

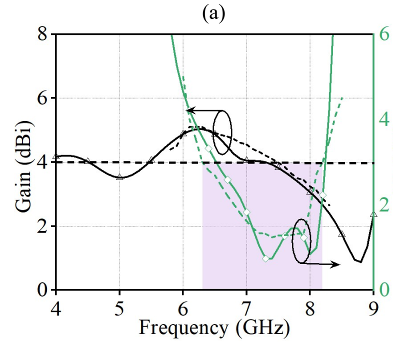

(b)

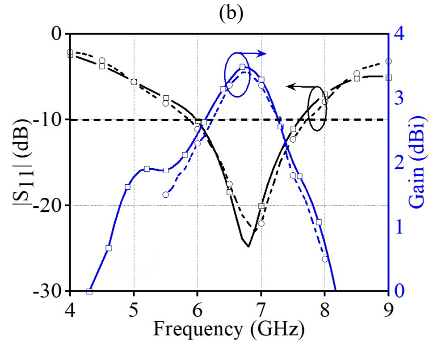

(c)

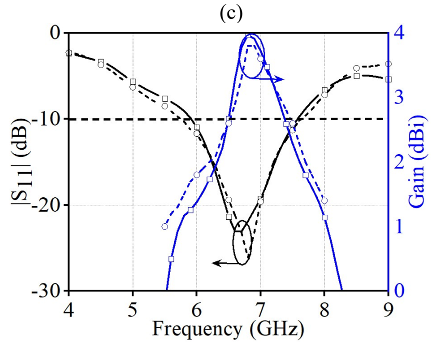

(d)

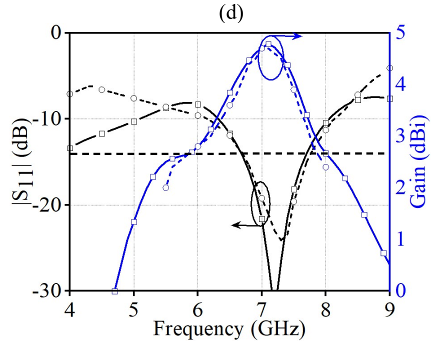

(e)

Fig. 10. The comparison of the simulated and measured results: (a) |S11| of the state 1, (b) AR and gain of the state 1, (c) |S11| and gain of the state 2, (d) |S11| and gain of the state 3, (e) |S11| and gain of the state 4.

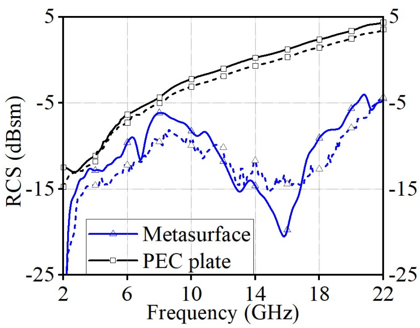

(a)

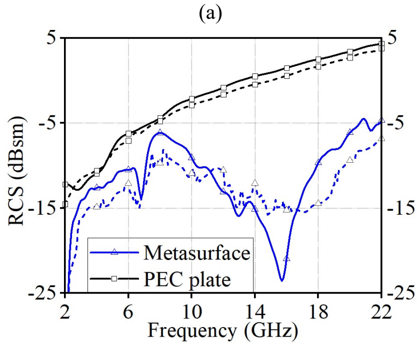

(b)

Fig. 11. Comparison of monostatic RCS between the proposed antenna and the copper plate for normal incident waves: (a) x-polarization and (b) y-polarization.

When switching from circular polarization (CP) to linear polarization (LP), the center frequency remains nearly constant, despite a reduction in bandwidth. Furthermore, the antenna demonstrates a low radar cross section (RCS) across the entire frequency band compared to a copper plate of the same size. It achieves an RCS reduction greater than 5 dBsm within the frequency range of 4.6 GHz to 22 GHz, corresponding to a bandwidth reduction of 130.8%, and a 6 dBsm reduction in RCS within the impedance bandwidth from 6.3 GHz to 7.2 GHz (13.3%), as illustrated in Fig. 11 (a) - (b). This indicates that the RCS of the metasurface antenna is considerably reduced within the specified frequency band. Fig. 12 shows the radiation patterns for four different states. (All solid lines are simulation, and all dotted lines are measurement.)

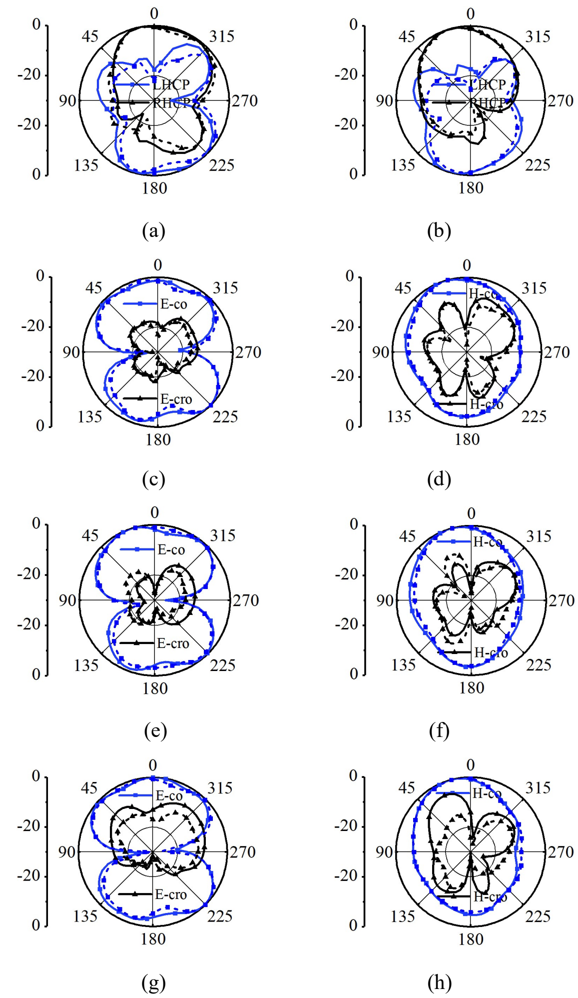

Fig. 12. The simulated and measured radiation patterns of the proposed antenna at 7 GHz: (a) xoz plane of the state 1 (LHCP and RLCP), (b) yoz plane of the state 1 (LHCP and RLCP), (c) xoz plane of the state 2, (d) yoz plane of the state 2, (e) xoz plane of the state 3, (f) yoz plane of the state 3, (g) xoz plane of the state 4, and (h) yoz plane of the state 4.

TABLE II
THE COMPARISON OF THE ANTENNA'S PERFORMANCES

Ref.	Profile (λ_0)	ARBW (%)	IBW (%)	PG (dBi)	Max. RE (%)	Components	Reconfigurable types
2024/[9]	0.03	1.5(RHCP) 1.6(RHCP)	5.1 (RHCP) 6.2 (RHCP)	4.40 4.80	90.0	2 capacitances	Frequency
2024/[14]	0.04	11.2	11.7 (CP) 11.6 (LP)	4.20 5.35	N. A	4 PINs and 3 inductances	Polarization
2021/[15]	0.21	N. A	18.1 (HP) 16.8 (VP)	2.04 1.10	70.8	Dielectric resonator	Polarization
2023/[19]	0.08	N. A	9.3 8.2	7.15 3.94	N. A	2 PINs	Pattern
2022/[20]	0.01	N. A	10.5	6.0	88.6	2 PINs	Pattern
2021/[26]	0.07	30.0	21.0 (HP) 22.0 (VP)	3.66 4.38	N. A	16 PINs	Polarization and pattern
This work	0.07	26.2	40.6 (CP) 26.5 (LP) 26.9 (LP) 26.9 (LP)	5.1 3.4 3.8 4.7	92.1 80.2 79.2 74.5	3 resistors	Polarization

Table II reports a comparison between the proposed antenna and several reconfigurable antennas, focusing on metrics such as profile, ARBW, IBW, PG, maximum RE, components, and reconfigurable types. The results show that most parameters for the proposed antenna exhibit superior performance. In contrast, using resistors for reconfigurable implementations is more practical, straightforward, and cost-effective.

IV. Conclusion

A low-profile, wideband metasurface CP antenna with reconfigurable and a low RCS has been designed, analyzed, and experimentally demonstrated. The MS design highlights the potential for achieving broadband performance, while the 90° rotation capability enables effective circular polarization. The combined metasurface and circular polarization techniques have been validated, highlighting their importance in the primary analysis and auxiliary design of the antenna. The proposed antenna features CP-to-LP switching, is cost-effective, and maintains a low profile with low RCS. These high-performance characteristics make it suitable for various modern wireless communication applications, including maritime and aviation mobile monitoring and broadcast frequency bands.

References

[1] Li L, Wu S, Pang D, Zhang X and Wang Q. A fifth-order single-layer dual-band half-mode SIW filtering antenna with a multifunctional single slot. *IEEE Antennas Wireless Propag. Lett.* 2021; 20(9): 1676-1680. https://doi.org/10.1109/LAWP.2021.3093062

[2] Yang S, Yan Z, Zhang T, Cai M, Fan F and Li X. Multifunctional tri-band dual-polarized antenna combining transmitarray and reflectarray. *IEEE Trans. Antennas Propag.* 2021; 69(9): 6016-6021. https://doi.org/10.1109/TAP.2021.3060938

[3] Cheng YJ, Tan FY, Zhou MM and Fan Y. Dual-polarized wideband plate array antenna with high polarization isolation and low cross polarization for D-band high-capacity wireless application. *IEEE Antennas Wireless Propag. Lett.* 2020; 19(12): 2023-2027. https://doi.org/10.1109/LAWP.2020.3020385

[4] Mohammadifar M, Mohammadi P, Zehforoosh Y. Printed dual-band base station antenna for GSM/DCS/PCS/UMTS and LTE applications with dual polarization. *Int J Circuit Theory Appl.* 2020;48(9):1544-1553. https://doi.org/10.1002/cta.2800

[5] Ding Z, Cao J, Yu J, Nasimuddin N, Chia MY, Tao S, Wang H. Low-profile miniaturized wideband circularly polarized monopole and MIMO antennas using characteristic mode analysis for wireless communication. *Radio Science* 2024; 59: e2024RS008030. https://doi.org/10.1029/2024RS008030

[6] M. Ciflik M, S. C. Basaran SC, O. Dandin O. Optically control tissue-independent reconfigurable antenna for body-centric communications at 2.4 GHz ISM band. *AEU-Int. J. Electron. Comm.* 2024; 178: 155304. https://doi.org/10.1016/j.aeue.2024.155304

[7] Xu G, Zhang X, Zhu L, Sun J, Mu W, Cao Q. A design of reconfigurable antenna with wide/narrow beam tunability. *AEU-Int. J. Electron. Comm.* 2024; 177: 155226. https://doi.org/10.1016/j.aeue.2024.155226

[8] Subbaraj S, Thomas SB. Reconfigurable antennas and their practical applications—A review. Radio Science 2023; 58: e2023RS007656. https://doi.org/10.1029/2023RS007656

[9] Han S, Wang Z and Dong Y. Miniaturized circularly polarized reconfigurable capacitance-loaded patch antenna. *IEEE Antennas Wireless Propag. Lett.* 2024; 23(4): 1226-1230. https://doi.org/10.1109/LAWP.2024.3349974

[10] Boukarkar A, Lin XQ, Jiang Y and Yang XF. A compact frequency-reconfigurable 36-states patch antenna for wireless applications. *IEEE Antennas Wireless Propag. Lett.* 2018; 17(7): 1349-1353. https://doi.org/10.1109/LAWP.2018.2846224

[11] Shirazi M, Huang J, Li T and Gong TX. A switchable-frequency slot-ring antenna element for designing a reconfigurable array. *IEEE Antennas Wireless Propag. Lett.* 2018; 17(2): 229-233. https://doi.org/10.1109/LAWP.2017.2781463

[12] Zadehparizi F and Jam S. Increasing reliability of frequency-reconfigurable antennas. *IEEE Antennas Wireless Propag. Lett.* 2018; 17(5): 920-923. https://doi.org/10.1109/LAWP.2018.2823688

[13] Han L, Wang C, Chen X and Zhang W. Compact frequency-reconfigurable slot antenna for wireless applications. *IEEE Antennas Wireless Propag. Lett.* 2016; 15: 1795-1798. https://doi.org/10.1109/LAWP.2016.2536778

[14] Jaiswal RX, Aakash, Ojha AK, Sim CYD and Srivastava KV. Wideband low-profile endfire antenna with polarization reconfigurability. *IEEE Trans. on Circuits Syst. II, Exp. Briefs* 2024; 71(4): 1984-1988. https://doi.org/10.1109/TCSII.2023.3334793

[15] Liu X, Leung KW and Yang N. Wideband horizontally polarized omnidirectional cylindrical dielectric resonator antenna for polarization reconfigurable design. *IEEE Trans. Antennas Propag.* 2021; 69(11): 7333-7342. https://doi.org/10.1109/TAP.2021.3076458

[16] Chen Q, Li JY, Yang G, Cao B and Zhang Z. A polarization-reconfigurable high-gain microstrip antenna. IEEE Trans. Antennas Propag. 2019; 67(5): 3461-3466. https://doi.org/10.1109/TAP.2019.2902750

[17] Bhattacharjee A, Dwari S and Mandal MK. Polarization-reconfigurable compact monopole antenna with wide effective bandwidth. *IEEE Antennas Wireless Propag. Lett.* 2019; 18(5): 1041-1045. https://doi.org/10.1109/LAWP.2019.2908661

[18] Cui Y, Qi C and Li R. A Low-Profile Broadband quad-polarization reconfigurable omnidirectional antenna. *IEEE Trans. Antennas Propag.* 2019; 67(6): 4178-4183. https://doi.org/10.1109/TAP.2019.2905987

[19] Tan S, Xiao Y, Liu Y, Liang Z, Li Y and Xu S. A pattern-reconfigurable endfire antenna based on compact folded slot with vertical polarization. *IEEE Antennas Wireless Propag. Lett.* 2023; 22(7): 1537-1541. https://doi.org/10.1109/LAWP.2023.3250322

[20] Zhao S, Wang Z and Dong Y. A planar pattern-reconfigurable antenna with stable radiation performance. *IEEE Antennas Wireless Propag. Lett.* 2022; 21(4): 784-788. https://doi.org/10.1109/LAWP.2022.3146599

[21] Yuan W, Huang J, Zhang X, Cui K, Wu W and Yuan N. Wideband pattern-reconfigurable antenna with switchable monopole and Vivaldi modes. *IEEE Antennas Wireless Propag. Lett.* 2023; 22(1): 199-203. https://doi.org/10.1109/LAWP.2022.3207199

[22] Fan C, Wu B, Hu Y, Zhao Y and Su T. Millimeter-wave pattern reconfigurable Vivaldi antenna using tunable resistor based on graphene. *IEEE Trans. Antennas Propag.* 2020; 68(6): 4939-4943. https://doi.org/10.1109/TAP.2019.2952639

[23] Yang G, Li J, Wei D, Zhou SG and Xu R. Pattern reconfigurable microstrip antenna with multidirectional beam for wireless communication. *IEEE Trans. Antennas Propag.* 2019; 67(3): 1910-1915. https://doi.org/10.1109/TAP.2018.2885230

[24] Li JF, Wu B, Zhou JQ, Guo KX, Zu HR and Su T. Frequency and pattern reconfigurable antenna using double layer petal shaped parasitic structure. *IEEE Trans. on Circuits Syst. II, Exp. Briefs* 2024; 71(4): 1934-1938. https://doi.org/10.1109/TCSII.2023.3329659

[25] Lv XL, Wu B, Fan C, Su T and Jiang D. Polarization/frequency hybrid reconfigurable microstrip antenna utilizing graphene-based tunable resistor. *IEEE Antennas Wireless Propag. Lett.* 2023; 22(2): 367-371. doi: 10.1109/LAWP.2022.3212885

[26] Nguyen-Trong N, Piotrowski A, Hall L and Fumeaux C. A frequency- and polarization-reconfigurable circular cavity antenna. *IEEE Antennas Wireless Propag. Lett.* 2017; 16: 999-1002. https://doi.org/10.1109/LAWP.2016.2616128

[27] Zainarry SNM, Nguyen-Trong N and Fumeaux C. A frequency- and pattern-reconfigurable two-element array antenna. *IEEE Antennas Wireless Propag. Lett.* 2018; 17(4): 617-620. https://doi.org/10.1109/LAWP.2018.2806355

[28] Yang J, Li J, Zhou S, Li D and Yang G. A polarization and frequency reconfigurable microstrip antenna for vehicular communication system application. *IEEE Trans. Veh. Technol.* 2023; 72(1): 623-631. https://doi.org/10.1109/TVT.2022.3202973

[29] Li T, et al. An ultrawideband low-loss reconfigurable metasurface element with 1-Bit resolution. *IEEE Antennas Wireless Propag. Lett.* 2024; 23(4): 1206-1210. https://doi.org/10.1109/LAWP.2023.3349290

[30] Yu J, Jiang W and Gong S. Low-RCS beam-steering antenna based on reconfigurable phase gradient metasurface. *IEEE Antennas Wireless*

Propag. Lett. 2019; 18(10): 2016-2020. https://doi.org/10.1109/LAWP.2019.2936300

[31] Li TJ, Wang GM, Guo WL, Xin KW, Han JQ and Li HP. Reconfigurable folded transmitarray antenna with low-profile based on metasurfaces. *IEEE Antennas Wireless Propag. Lett.* 2023; 22(3): 611-615. https://doi.org/10.1109/LAWP.2022.3219994

[32] Li W, Wang YM, Hei Y, Li B and Shi X. A compact low-profile reconfigurable metasurface antenna with polarization and pattern diversities. *IEEE Antennas Wireless Propag. Lett.* 2021; 20(7): 1170-1174. https://doi.org/10.1109/LAWP.2021.3074639

[33] Li L, Yan X, Zhang HC and Wang Q. Polarization- and frequency-reconfigurable patch antenna using gravity-controlled liquid metal. *IEEE Trans. on Circuits Syst. II, Exp. Briefs* 2022; 69(3): 1029-1033. https://doi.org/10.1109/TCSII.2021.3119040

[34] Liu Y, Wang Q, Jia Y and Zhu P. A frequency- and polarization-reconfigurable slot antenna using liquid metal. *IEEE Trans. Antennas Propag.* 2020; 68(11): 7630-7635. https://doi.org/10.1109/TAP.2020.2993110

[35] Wang P, Jia Y, Liu Y and Hu W. A wideband low-RCS circularly polarized reconfigurable C-shaped antenna array based on liquid metal. *IEEE Trans. Antennas Propag.* 2022; 70(9): 8020-8029. https://doi.org/10.1109/TAP.2022.3164179

[36] Harrington R, Mautz J and Chang Y. Characteristic modes for dielectric and magnetic bodies. *IEEE Trans. Antennas Propag.* 1972; 20(2): 194-198. https://doi.org/10.1109/TAP.1972.1140154

[37] Harrington R and Mautz J. Theory of characteristic modes for conducting bodies. *IEEE Trans. Antennas Propag.* 1971; 19(5): 622-628. https://doi.org/10.1109/TAP.1971.1139999

[38] Knorr J. Consequences of symmetry in the computation of characteristic modes for conducting bodies. *IEEE Trans. Antennas Propag.* 1973; 21(6): 899-902. https://doi.org/10.1109/TAP.1973.1140622